Radiation chemistry in ammonia-water ices

M. J. Loeffler,[1,2,a)] U. Raut,[2] and R. A. Baragiola[2]
[1]*Astrochemistry Laboratory, NASA GSFC, Code 691, Greenbelt, Maryland 20775, USA*
[2]*Laboratory for Atomic and Surface Physics, Engineering Physics, University of Virginia, Charlottesville, Virginia 22904, USA*

(Received 3 October 2009; accepted 13 January 2010; published online 4 February 2010)

We studied the effects of 100 keV proton irradiation on films of ammonia-water mixtures between 20 and 120 K. Irradiation destroys ammonia, leading to the formation and trapping of H_2, N_2, NO, and N_2O, the formation of cavities containing radiolytic gases, and ejection of molecules by sputtering. Using infrared spectroscopy, we show that at all temperatures the destruction of ammonia is substantial, but at higher temperatures (120 K), it is nearly complete (~97% destroyed) after a fluence of 10^{16} ions/cm^2. Using mass spectroscopy and microbalance gravimetry, we measure the sputtering yield of our sample and the main components of the sputtered flux. We find that the sputtering yield depends on fluence. At low temperatures, the yield is very low initially and increases quadratically with fluence, while at 120 K the yield is constant and higher initially. The increase in the sputtering yield with fluence is explained by the formation and trapping of the ammonia decay products, N_2 and H_2, which are seen to be ejected from the ice at all temperatures. © *2010 American Institute of Physics*. [doi:10.1063/1.3308484]

I. INTRODUCTION

The equilibrium phase diagram of the ammonia-water system shows that hydrated $H_2O:NH_3$ compounds form in the ratios 1:2 (hemihydrate), 1:1 (monohydrate), and 2:1 (dihydrate).[1] In the solid phase, these different hydrates have distinct crystal structures and infrared (IR) absorption spectra.[2,3] These mixtures are almost certainly present in comets[4] and in grains in the atmospheres of the giant planets. Ammonia was predicted to exist in icy satellites in the outer solar system.[5,6] Since ammonia lowers the melting point of water drastically, by ~100 K, it could allow cryovolcanism in icy satellites around Saturn and Uranus.[7] An erupting subsurface liquid may be the source of the spectacular polar plumes in the Saturnian moon Enceladus.[8] The presence of ammonia in Enceladus has been discussed, for instance, by Kargel and Pozio[9] and deduced by Ostro[10] from radar backscattering observations, and used by Stegman *et al.*[11] to propose a double layer subsurface ocean with water below and ammonia dihydrate on top. The most recent evidence for the presence of ammonia is its detection in Enceladus' plume by Cassini's mass spectrometer (MS).[12]

However, ammonia has only been identified in the IR reflectance spectra of Charon[13] and possibly a few other icy satellites,[14] using a very weak feature in their near IR reflectance spectra. A leading explanation for the discrepancy between expectations and observations is that ammonia is quickly depleted from the surface by energetic ion irradiation[15] with respect to the bulk of the ice, where radiation would not penetrate. This was based on experiments that showed that the sputtering yield of pure solid ammonia under 1.5 MeV He^+ bombardment is ~18 times higher than it is for water ice. Those initial studies on pure ammonia have been recently extended to the more relevant case of ammonia-water mixtures,[3,16,17] which show ion irradiation indeed depletes ammonia preferentially relative to water ice. In particular, Loeffler *et al.*[16] have discussed the experiments in relation to the small surface abundance of NH_3 at Enceladus, and proposed that radiolysis plus heating can cause the explosive desorption of nitrogen, hydrogen, and ice particles, and act as a source of N^+ detected on the magnetosphere of Saturn, peaking around Enceladus' orbit.[18]

In addition to these astronomical applications, there is a basic interest in radiolysis of this simple binary mixture with only three types of atoms: H, N, and O. Irradiation of pure water ice produces unstable radicals (H, O, OH, and HO_2) and minor amounts of stable molecular products (H_2, O_2, and H_2O_2), leaving most of the H_2O intact. In contrast, radiolysis of pure ammonia leads to the eventual disintegration into N_2 and H_2 through reactions involving radicals H, NH, and NH_2 (Refs. 19 and 20) and small transient quantities of N_2H_4, N_2H_2, and HN_3.[20] Irradiation of ammonia-water mixtures results in reactions between the two groups of radicals, leading to the formation of new species such as N_xO_y, which has been shown previously for ion irradiation of N_2–H_2O mixtures.[21] In the experiments presented here, we studied 100 keV proton irradiation of 1:2 ammonia-water mixtures at 20, 70, and 120 K using a distinctive combination of characterization techniques: IR spectroscopy, mass spectrometry, and microgravimetry that allowed the quantification of the chemical composition of the solid and sputtered species as a function of irradiation fluence.

II. EXPERIMENTAL SETUP

All experiments were performed in a cryopumped stainless-steel vacuum chamber on a radiation-shielded cryostat (for more details see Ref. 22). The base pressure of the

a)Electronic mail: mark.loeffler@nasa.gov.

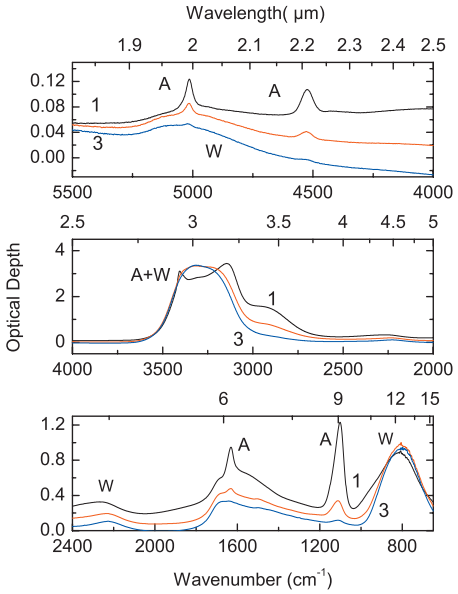

FIG. 1. IR absorption spectra of a 1:2 ammonia-water mixture at 120 K before (1) and after (2) 1.8×10^{15} ions/cm^2 and (3) 7.1×10^{15} ions/cm^2. We have denoted water as W and ammonia as A.

chamber was $\sim10^{-10}$ Torr and 1–2 orders of magnitude lower inside the shield. Solid ammonia-water films were grown at 80 K by vapor deposition on an optically flat gold mirror electrode of a 6 MHz quartz-crystal microbalance. The areal mass Q (mass/area) of the films was determined by the change in the resonance frequency of the crystal, which was measured with an Inficon IC/5 controller to a resolution of 0.1 Hz.[23] The measured Q can be converted to film column density η (molecules/cm^2) if the film composition is known, and converted to thickness if the mass density is known.[23]

The films deposited had 148 μg/cm^2 [~2 μm], slightly larger than the depth of penetration of the 100 keV H^+ ions at 9° incidence used during irradiation.[24] These mixtures were grown using two separate gas dosers adjusting the relative gas fluxes to achieve the 1:2 NH_3:H_2O ratio of the dihydrate, one of the equilibrium phases for ice mixtures with $<$65.4 wt % ammonia.[5] After growth, the films were warmed to 120 K to achieve uniform mixing and subsequently cooled to 20, 70, or 120 K where the irradiation was performed.

The proton beams used in these experiments were produced by an ion accelerator, mass analyzed and scanned uniformly over the film. A thin wire collector placed in the ion beam path, and calibrated against a Faraday cup, monitored the proton current and fluence. A new calibration from our laboratory showed that previous measurements of fluence in papers reported in the past two years[22,25–27] were too high by 25%. A Dycor M200 quadrupole MS monitored the species ejected (sputtered) during irradiation or desorbed during heating of the film. This temperature programmed desorption study was done at 0.2 K/min.

The specular reflectance of the films on the gold mirror was measured in the IR at an incident angle of 35°. The spectra were recorded with a Thermo-Nicolet Nexus 670 Fourier transform IR spectrometer at 2 cm^{-1} resolution. The

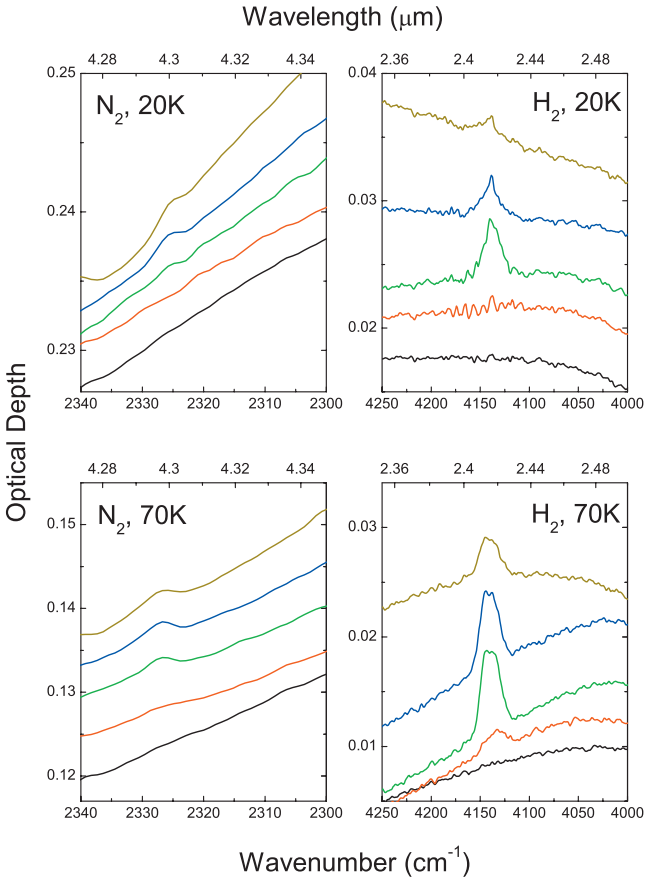

FIG. 2. IR spectra of N_2 (left) and H_2 (right) formed during ion irradiation of a 1:2 ammonia-water mixture irradiated with 100 keV protons at 20 K (bottom) and 70 K (top). Fluences in top panels from top to bottom are: 0, 0.028, 0.38, 2.1, and 8.3×10^{15} ions/cm^2. Fluences in bottom panels are: 0, 0.11, 1.1, 2.4, and 9.8×10^{15} ions/cm^2.

spectra were divided by the reflectance of the gold mirror substrate taken before film deposition. The ratios $R(\lambda)$ were then converted to optical depth units, $-\ln R(\lambda)$. Absorption band areas (BAs) were derived after subtraction of baselines that matched the continuum at both sides of the bands. In Fig. 1, we show our IR spectra of the ammonia-water mixture before and after irradiation with 100 keV protons at 120 K.

III. RESULTS

A. IR spectroscopy

As is seen in Fig. 1, the IR spectrum before and after irradiation is dominated by water and ammonia features. However as we irradiate the sample, we observe the appearance of new absorption bands in the spectrum (Figs. 2 and 3). At 20 and 70 K, small bands emerge at 4139 cm^{-1} (H_2) and 2325 cm^{-1} (N_2), while a band at 1505 cm^{-1} (NH_4^+ (Ref. 3), NH_2^- (Ref. 28) or possibly the NH_2 radical (Ref. 29)) appears at all temperatures. In addition, at 20 K we also observe bands at 3671 cm^{-1} [OH dangling bonds (DBs) at internal surfaces of micropores] and 1872 cm^{-1} (NO; Ref. 30), while we observe N_2O (2225 cm^{-1}; Ref. 30) only at 120 K. The appearance, at 20 and 70 K, of dipole absorption bands of H_2 and N_2, forbidden for free molecules is likely due to symmetry breaking perturbations at defect sites

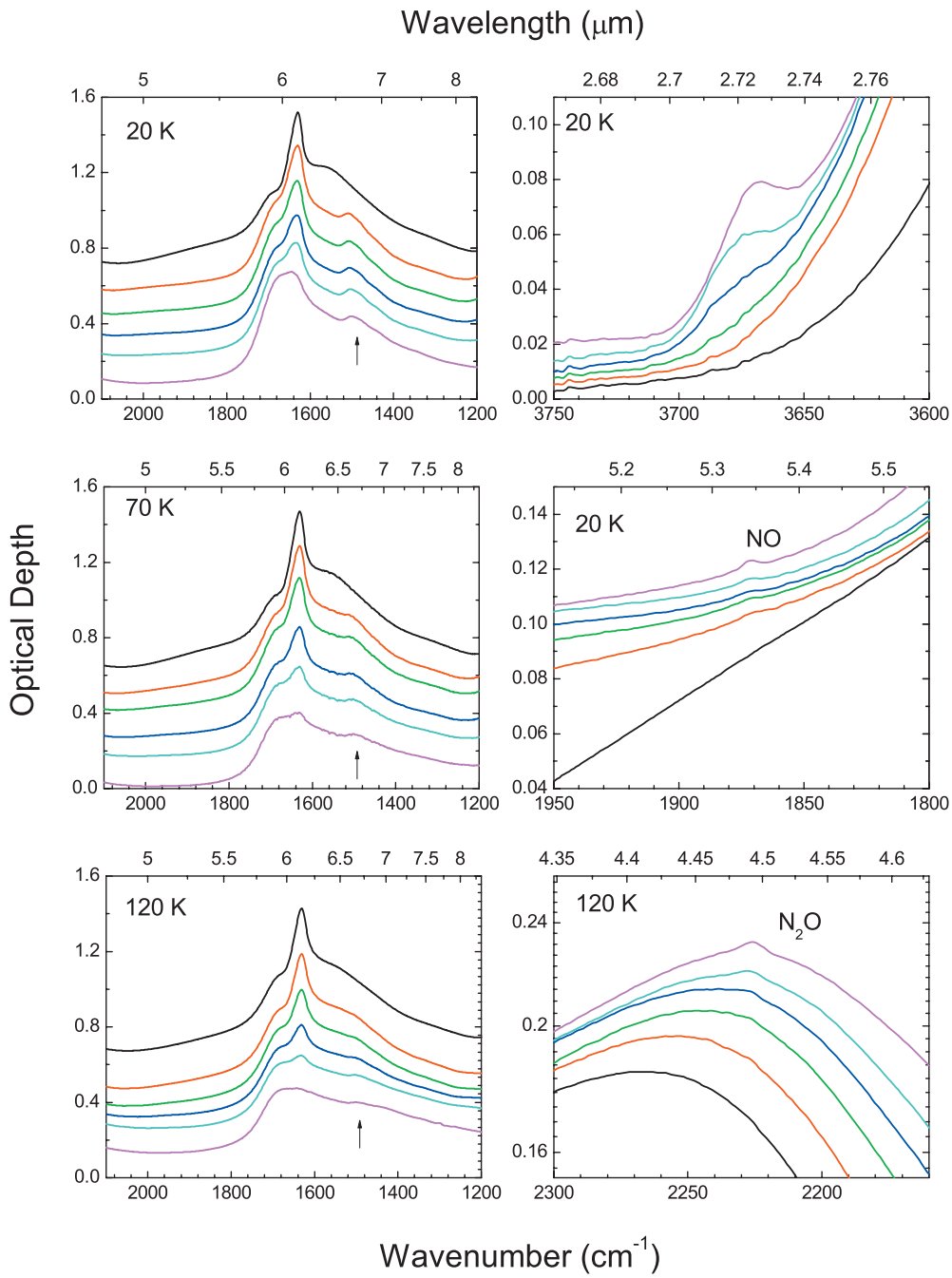

FIG. 3. IR spectra for minor species: NH_4^+ or NH_2^- (all temperatures; left panel), DBs (20 K; top right panel), NO (20 K, middle right panel), and N_2O (120 K, bottom right panel). Fluences in top and bottom left panels from top to bottom are: 0, 0.20, 0.58, 1.1, 2.2, and 8.3 ($\times 10^{15}$ ions/cm^2). Fluences in middle left panel are: 0, 0.20, 0.58, 1.41, 2.4, and 8.3 ($\times 10^{15}$ ions/cm^2). Fluences in all the right panels are from bottom to top: 0, 0.20, 0.58, 1.1, 2.2, and 8.3 ($\times 10^{15}$ ions/cm^2).

(e.g., molecules trapped at vacancies). Figures 4 and 5 show the fluence dependence of the IR absorption BA of different molecules and of the DBs. The ammonia band at 4523 cm^{-1} decreases monotonically with fluence while the other bands grow to a steady state at high fluences whereas the signal for H_2 grows to a peak and decays.

B. Sputtering

In Fig. 6, we plot the fluence dependence of the total mass loss and the sputtering yield, the average number of molecules ejected per ion. In the case of the irradiation at 120 K, initially there was some slow outgassing of ammonia: 7×10^{13} NH_3/cm^2 s, that was below the background of the MS. We subtracted this contribution from the mass loss due to sputtering. To derive sputtering yield from a mass loss we divide by 28 amu, since N_2 is the main constituent of the sputtered flux. In Fig. 7 we show N, rather than N_2, because of a better signal to noise ratio. The ratio of intensities of N to N_2 is about 15%, consistent with the ratio obtained by fragmentation of N_2 in the MS. Since the sputtering of water ice is quite smaller than that of ammonia[31] it becomes significant only for the very low rates of mass loss at high fluence. Sputtering of ammonia molecules cannot be mea-

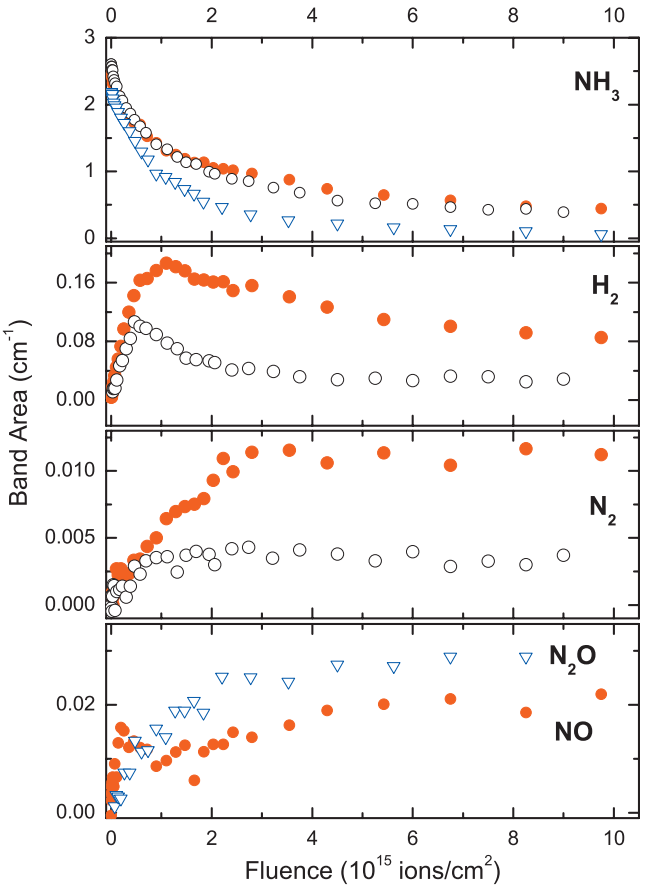

FIG. 4. Fluence dependence of the IR absorption of new molecular species at different temperatures during irradiation of a 1:2 ammonia-water mixture. Full symbols: 20 K, open circles: 70 K, and triangles: 120 K. Top: destruction of ammonia, second panel: formation of H_2, third panel: formation of N_2, bottom: formation of NO and N_2O.

sured directly because of interference with background OH. We tried to measure sputtered ammonia from the expected fragments, NH and NH_2, produced in the MS, but the signal at those masses was below the noise level, indicating that ejection of intact NH_3 molecules is at most a minor contributor to sputtering. A similar conclusion can be reached from the small initial sputtering yield, when the film contains only

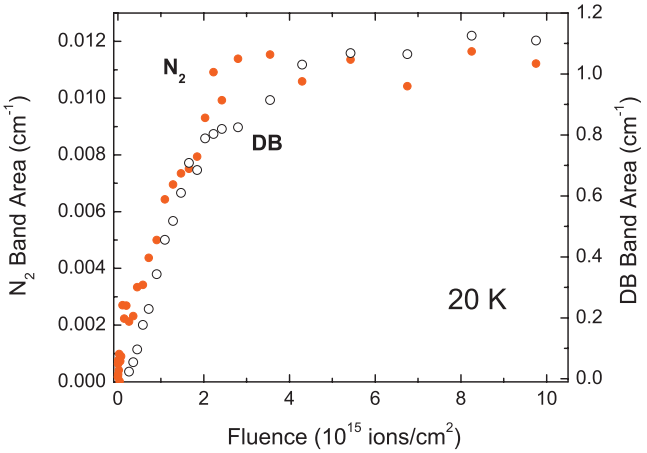

FIG. 5. Fluence dependence of the formation of N_2 (●) and DB (○) absorptions as indicated by IR spectroscopy in a 1:2 ammonia-water mixture during irradiation with 100 keV H^+ ions at 20 K.

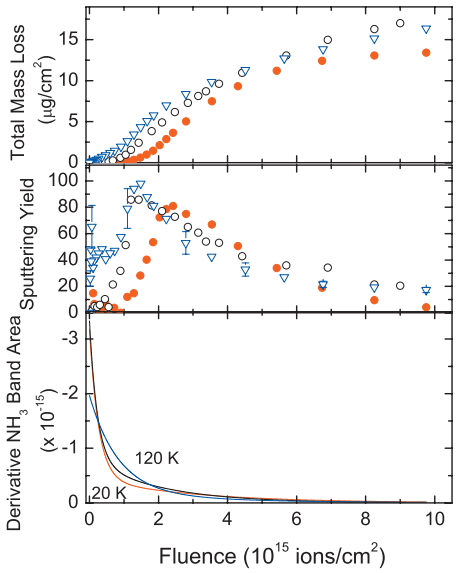

FIG. 6. Total mass loss (top) and sputtering yield (mass loss divided by 28 amu) (middle) and smoothed derivative of the calculated NH_3 BA shown in Fig. 4 (bottom) of a 1:2 ammonia-water mixture during irradiation with 100 keV protons as a function of fluence at 20 K (●), 70 K (○), and 120 K (▽).

water and ammonia. These results are consistent with previous MS studies on irradiation of solid ammonia with low energy (3 keV) ions,[32] which showed that ions with a significant electronic stopping component, such as in the experiments reported here, sputter predominantly H_2 and N_2, with a flux that is approximately an order of magnitude higher than that of sputtered NH_3

The shape of the total mass loss curve shows an interesting initial behavior, as at lower temperatures the initial rise is delayed to higher fluences. The effect of sputtering is seen more clearly when we calculate the sputtering yield (Fig. 6, middle), from the derivative of the top panel. For low fluences, the yield is constant (~45) at 120 K whereas at lower temperatures the yield starts very small and rises qua-

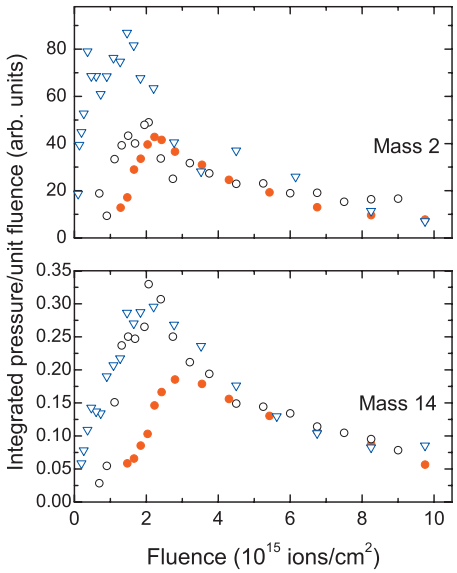

FIG. 7. MS reading during sputtering for 2 (top) and 14 (bottom) amu during irradiation of a 1:2 ammonia-water mixture at 20 K (●), 70 K (○), and 120 K (▽).

dratically with fluence. The sputtering yield goes through a peak and decays at high fluences to values similar to the sputtering yield of pure water ice.[31] Furthermore, while the fluence dependence is a strong function of temperature, the maximum value of the yield is not.

The fluxes of ejected H_2 and N measured by the MS increase with fluence, peak, and then fall at high fluences. At all temperatures the peak of N sputtering and of the total yield occurs at the same fluence: $\sim 3 \times 10^{15}$ ions/cm^2 at 20 K and $\sim 2 \times 10^{15}$ ions/cm^2 at 70 and 120 K. The ejection of hydrogen also peaks at higher fluences at the lowest temperature, while the intensity increases with increasing temperature. As we noted above, the variations in hydrogen sputtering will not affect significantly the total sputtering yield measurements, since hydrogen is much lighter than the other sputtered species.

IV. DISCUSSION

A. Radiochemical pathways

The radiation chemistry of ammonia-water mixtures involves dozens of ionic and neutral species, and hundreds of potential different reactions among them. An in-depth analysis is therefore not possible without drastic simplifications, and thus we will restrict the discussion to reactions that can explain the observed fluence and temperature dependence of the chemical composition of the films and of the sputtered flux.

The basic physics and chemistry of radiolysis, together with main reaction channels are described in Spinks and Woods,[33] although most of the data presented refer to pure substances in the gas phase. Radiolysis starts with ionizations, excitations, and dissociations by the projectiles and secondary electrons. We discuss first ionic species (ions and electrons), which are typically more than half the primary products. The charges are balanced and the solid remains neutral, except for the escape of electrons into vacuum and charge transfer at the film/substrate interface. At temperatures below 100 K, electrons move freely in the conduction band, but at higher temperatures, they can self-trap, which is assisted by lattice fluctuations and the surrounding solvation shell of polarized molecules. Ions are relatively immobile at low temperatures and trap readily, again polarizing the surrounding medium. An example is the protonated water cluster solvated due to the polarization of the medium around the ion, in a process that releases a hydroxyl radical

$$H_2O^+ + (H_2O)_n \rightarrow H^+(H_2O)_n + OH. \quad (1)$$

Neutralization of positive ions with electrons occurs mostly by dissociative recombination, a process much faster than radiative recombination. The kinetic energy that is carried by the products can lead to lattice defects and sputtering. Another recombination channel is the interaction of positive and negative ions, which is much slower due to the lower mobility of negative ions compared to electrons, particularly at cryogenic temperatures.

Neutral dissociation products can form directly in dissociation collisions. The main channels for water and ammonia are (X denotes the projectile ion or an energetic secondary electron)

$$H_2O + X \rightarrow H + OH, \quad (2)$$

$$H_2O + X \rightarrow H_2 + O \text{ or } 2H + O, \quad (3)$$

$$NH_3 + X \rightarrow H + NH_2, \quad (4)$$

$$NH_3 + X \rightarrow H_2 + NH. \quad (5)$$

These reactions therefore produce, as primary products, H, O, OH, H_2, NH, and NH_2. If the collisions occur in a dilute gas, then the products will escape the collision region and never collide again. In the condensed state, there is a large probability that the products collide with the surrounding molecules (the "cage") and reform the original molecule (geminate recombination). Thus, the radiation yields G, number of products formed by 100 eV of deposited energy, are several times smaller in the condensed phase than for free molecules. With increasing temperature, the cage becomes more pliable, and cage escape becomes increasingly important, producing an increase in G with temperature. Cage escape is more likely for H than for the heavier atoms or molecular products, such as O, OH, NH_2, etc.

An important mechanism is intratrack reactions between radicals and molecules in the ion track. The clearest evidence for this process is the linear production of N_2 molecules with irradiation fluence, which requires two N atoms from two separate collisions. This behavior is not possible in UV photolysis where a photon can only produce one dissociation upon absorption.

In a dissociation process, the lighter product carries most of the kinetic energy due to conservation of momentum. This effect, plus the reduced interaction cross sections, cause H atoms to leave the cage and diffuse in the solid, where they can recombine to form H_2, which can escape the solid, be trapped at radiation defects (for a discussion on radiolysis of water ice, see Ref. 34), or react with other radicals which may have accumulated in the solid.

As a result of dissociations, ion-molecule reactions, and DR processes, the solid will contain a time-dependent concentration of radicals (e.g., H, O, OH, NH, etc.) and stable molecules (H_2O, NH_3, O_2, H_2, etc.) with a concentration that depends on the relative importance of different reactions.

In the ammonia dihydrate, radiolysis will not just be a superposition of radiation effects of water and ammonia, since there will be cross reactions between different radicals. This is demonstrated by the observation of NO and N_2O. Another important consequence of the presence of water is the much larger yield for destruction of ammonia in comparison with the case of pure solid ammonia, as recently demonstrated by Moore *et al.*[3]

Among the potential reactions of ammonia with water radiation products are these ionization channels

$$H_3O^+ + NH_3 \rightarrow NH_4^+ + H_2O, \quad (6)$$

$$NH_3^+ + H_2O \rightarrow NH_4^+ + OH. \quad (7)$$

However, the ammonium ion can be neutralized and rebuild NH_3 by, for example

$$e^- + NH_4^+ \rightarrow NH_3 + H, \quad (8)$$

$$NH_2^- + NH_4^+ \rightarrow 2NH_3, \quad (9)$$

where NH_2^- can be formed by dissociative electron attachment to NH_3. As judged from measurements on an Ar matrix, and considering possible redshifts in the water matrix, both NH_2^- and NH_4^+ can be responsible for the small 1505 cm^{-1} band in our spectra.[3,28,29]

We will now propose different channels that could account for the increased destruction of ammonia in aqueous solutions and the results presented above. Both the additional H from dissociation of water and the reactions with NH_4^+ mentioned above will reform NH_3 from NH_2, its main dissociation product. We thus propose that destruction of NH_3 is strongly favored by reactions with OH and O, which deplete those radicals thus explaining the absence of H_2O_2 and O_2 in our experiments:

$$NH_3 + OH \rightarrow NH_2 + H_2O, \quad (10)$$

$$NH_3 + O \rightarrow NH_2 + OH, \quad (11)$$

$$NH_2 + O \rightarrow NH + OH, \quad (12)$$

$$NH + NH \rightarrow N_2H_2 \rightarrow N_2 + H_2. \quad (13)$$

Reaction (13) occurs since N_2H_2 is unstable[35] and explains the formation of both H_2 and N_2 in addition to reaction (5) that produces H_2.

The NO and N_2O molecules can be formed through the oxidation reactions, such as

$$OH + NH_3 \rightarrow H_2O + NO, \quad (14)$$

$$OH + NH \rightarrow H_2 + NO, \quad (15)$$

$$O + NH \rightarrow NO + H, \quad (16)$$

$$O + NH_2 \rightarrow NO + H_2, \quad (17)$$

$$N + NO \rightarrow N_2O. \quad (18)$$

This last reaction explains the formation of N_2O at higher temperatures, which is enabled by N diffusion.

Other products such as hydrazine could feasibly form by similar reaction mechanisms but be mostly destroyed by radicals, such as in

$$H + N_2H_4 \rightarrow H_2 + N_2H_3, \quad (19)$$

$$NH_2 + N_2H_4 \rightarrow NH_3 + N_2H_3, \quad (20)$$

followed by other reactions that end in H_2 and N_2. However, we note that such products would be very difficult to detect with IR spectroscopy because their absorptions overlap with other stronger bands.

B. DB formation

As shown in Fig. 3 (top right), we observed the formation of an absorption band (OH stretch) at 3671 cm^{-1} due to DBs of water after irradiation at 20 K but not at 70 or 120 K. These DBs have also been shown to form during ion irradiation of hydrogen peroxide at 17 K.[22] The DB absorption indicates the presence of pores or cavities with large internal surface areas.[36,37] When the pores contain adsorbed gas, the DB band is shifted with respect to that of pure ice (3692 cm^{-1}).[36,37] In our experiment, the absorbed gas is likely nitrogen since the DB absorption band is located at ~3676 cm^{-1}, which is similar to that reported for water ice codeposited with nitrogen.[36] The existence of gas-filled cavities as a consequence of radiation damage is a well-studied phenomenon in nuclear reactors and has been proposed to occur in icy satellites.[38] The basic mechanism is the formation of defects by displacement collisions, their coalescence in voids, which are stabilized by the gas. We note that in pure water ice, the concentration of molecular products (H_2 and O_2) is too small to produce sufficient voids to produce a measurable DB signal. This is likely why in ion irradiation experiments of pure water ice DB present in the initially porous sample are quickly destroyed.[27,39]

C. Identification of the 1505 cm^{-1} band

We noted that the absorption band at 1505 cm^{-1} could either be due to NH_2, NH_4^+ or the NH_2 radical. In our experiments, we find that the feature is produced at all temperatures and remains in the ice until the sample begins to crystallize (130–140 K). Thus, we conclude it is most likely due to ions that should be rather immobile due to their solvation shell. The instability of the NH_2 radical is supported by previous measurements,[29] that showed that the absorption feature of NH_2 disappears when the sample was warmed to 35 K, indicating that the radical reacted with other molecules in the matrix.

D. Temperature dependence of IR absorption of H_2 and N_2

The mass loss measured by the microbalance during the course of this experiment shows that <30% of the ammonia is removed by ion impact (sputtering). Thus, the drop of 85% (20 K)—97% (120 K) in the NH_3 IR BA is due to the decomposition of the molecule and formation of radiation products trapped in the ice, that include H_2 and N_2 (Fig. 2).

As mentioned, the IR BA of the dipole forbidden transitions of H_2 and N_2 are greater at 20 K than at 70 K and are undetectable at 120 K. This observation may imply lower amounts are trapped as the temperature is increased. However, since the absorption strength of these transitions, which are forbidden in the gas phase, is very sensitive to perturbations,[40] the decrease in band intensity could also be explained by the migration of synthesized molecules from traps into clusters or gas bubbles[16,22,38] where they are less

perturbed and therefore less likely to absorb IR light. As we will see later, aggregation of molecules has a bearing on the sputtering results.

E. Quantification of ammonia destruction

We can quantify the destruction of ammonia using the initial slope of the evolution of the column density with fluence, $d\eta/dF$. We obtain $\eta(F)$ as the product of the IR BA in Fig. 4 by the value of η/BA at zero fluence. From the initial slope, we can calculate the radiation yield G, defined as the initial number of products produced or destroyed per 100 eV of energy absorbed. The values for $G(-NH_3)=(d\eta/dF)\times(100\ \mathrm{eV}/\Delta E)$, where $\Delta E=100$ keV, are similar at 20 K (2.3) and 70 K (2.4) and significantly lower at 120 K (1.5). The $G(-NH_3)$ value of the dihydrate at 70 K is ~8 times larger than for pure ammonia irradiated with electrons at 77 K.[19] We note that even though the initial slope $d\eta/dF$ is larger at the lower temperatures, the equilibrium η at high fluences is lowest in the sample irradiated at 120 K, which indicates that reformation of NH_3 is inefficient at this temperature, likely due to enhanced formation and outdiffusion of H_2.

F. Sputtering

We now turn to the discussion of sputtering. First, we recall some known facts and concepts:

(1) The total mass loss rate is dominated by species containing nitrogen due to the low mass of hydrogen.
(2) Since sputtering removes only ~10% of the film during the experiment, its effect in total column density of molecules is small.
(3) Sputtering involves only a shallow surface layer (<a few nm) due to the limited range of the recoiling molecules in the solid. Therefore, the yield of molecules emitted reflects the composition of the surface rather than that of the bulk, which contributes to the signal observed in IR spectroscopy.
(4) Since mass loss at 20 and 70 K stops when the ion beam is turned off thermal desorption is negligible except, possibly, for H_2. The slow outgassing at 120 K, mentioned above, will be enhanced with the beam on by the process of radiation-enhanced diffusion, which increases with temperature.

We note that, at 20 and 70 K, but not at 120 K, sputtering of nitrogen and hydrogen grows initially with the square of fluence, passes through a maximum, and decays exponentially (Fig. 7). The initial square dependence may seem surprising since the N_2 column density in the film grows linearly with fluence (Fig. 4). However, sputtering depends on the surface concentration, which is different from the bulk due to preferential sputtering. The initial quadratic growth suggests that a pair of molecules is needed to produce sputtering, such aggregation into pairs will also occur in the bulk without affecting the IR signal significantly. Aggregation requires diffusion, which can be induced by the ions at the lower temperatures where thermal diffusion is slow. This behavior is similar to what happens with irradiation of water, where Teolis *et al.*[41] have shown that diffusion of O_2 radiation products from water is suppressed at 20 K. Radiation enhanced diffusion increases with temperature, which explains the faster initial square growth at 70 K than at 20 K. The situation is different at 120 K, where thermal diffusion is important and explains why sputtering of nitrogen starts immediately, as shown in Fig. 6.

At high fluences, sputtering decreases exponentially, which is attributed to depletion of the surface concentration of N_2 by preferential sputtering. Finally, we note that the intensity of ejected H_2 is similar at 20 and 70 K and almost a factor of two higher at 120 K, indicating that the ice is much less efficient in trapping hydrogen at the higher temperatures.

G. Astrophysical implications: Charon and Enceladus

The flux and composition of radiation incident on an object can vary significantly depending on its location in the solar system. The primary component impacting Charon is protons; their flux and corresponding energy dosage[42] suggest that ~40% of the ammonia originally present will be lost from the surface over the moon's lifetime (~4.5 Ga). We note this predicted loss may be an underestimate, since previous models did not take into account heavier less abundant ions, which have played a significant role on the radiation effects in other environments, such as the interstellar medium.[26,43]

On Enceladus, which has a more intense radiation environment that is dominated by energetic electrons,[44] it should take only $\sim 10^4$ years to bring the ammonia feature down to the noise level of the current observations, in agreement with previous laboratory estimates.[3] We note that this timescale is much longer than our previous estimate, given as a lower limit.[16] This discrepancy results from recent reports by the Cassini Magnetospheric Imaging Instrument[45] that show the radiation flux data obtained from Voyager missions[46] were too high, although a large variation cannot be discarded in the time between Voyager and Cassini.

V. CONCLUSIONS

Irradiation of ammonia-water mixtures by 100 keV protons between 20 and 120 K destroys 80% or more of the ammonia, forming N_2 and H_2 and minor amounts of N_2O (120 K) and NO (20 K), which are trapped at defects in the ice. The appearance of IR absorption of DBs in the ice at 20 K indicates the formation of cavities which are likely stabilized by the trapped hydrogen and nitrogen in the sample.

The sputtering yield at 20 and 70 K begins very low and increases quadratically with fluence. In contrast, at 120 K the initial sputtering yield is relatively high and constant. The sputtering yield peaks at a value that is approximately independent on temperature, while the fluence at which the yields peak decrease with increasing temperature. This fluence dependence in the sputtering yield is explained by the formation, trapping, and subsequent removal of the ammonia decay products—N_2 and H_2.

ACKNOWLEDGMENTS

This research was supported by Grant No. NNX07AL48G from NASA Outer Planet Research and Grant No. NNX08AMB6G from Planetary Geology and Geophysics programs. We thank Dr. J-H. Kim for calibration of the beam current monitor.

[1] J. S. Kargel, Icarus **100**, 556 (1992).
[2] J. S. Holt, D. Sadoskas, and C. J. Pursell, J. Chem. Phys. **120**, 7153 (2004); J. E. Bertie and M. R. Shehata, *ibid.* **83**, 1449 (1985); **81**, 27 (1984).
[3] M. H. Moore, R. F. Ferrante, R. L. Hudson, and J. N. Stone, Icarus **190**, 260 (2007).
[4] H. Kawakita and J.-i. Watanabe, Astrophys. J. **572**, L177 (2002).
[5] D. L. Hogenboom, J. S. Kargel, G. J. Consolmagno, T. C. Holden, L. Lee, and M. Buyyounouski, Icarus **128**, 171 (1997).
[6] J. S. Lewis, Icarus **16**, 241 (1972); D. J. Stevenson, Nature (London) **298**, 142 (1982).
[7] J. S. Kargel, Earth, Moon, Planets **67**, 101 (1994).
[8] C. C. Porco, P. Helfenstein, P. C. Thomas, A. P. Ingersoll, J. Wisdom, R. West, G. Neukum, T. Denk, R. Wagner, T. Roatsch, S. Kieffer, E. Turtle, A. McEwen, T. V. Johnson, J. Rathbun, J. Veverka, D. Wilson, J. Perry, J. Spitale, A. Brahic, J. A. Burns, A. D. DelGenio, L. Dones, C. D. Murray, and S. Squyres, Science **311**, 1393 (2006).
[9] J. S. Kargel and S. Pozio, Icarus **119**, 385 (1996).
[10] S. J. Ostro, Icarus **183**, 479 (2006).
[11] D. R. Stegman, J. Freeman, and D. A. May, Icarus **202**, 669 (2009).
[12] J. H. Waite, W. S. Lewis, B. A. Magee, J. I. Lunine, W. B. McKinnon, C. R. Glein, O. Mousis, D. T. Young, T. Brockwell, J. Westlake, M.-J. Nguyen, B. D. Teolis, H. B. Niemann, R. L. McNutt, Jr., M. Perry, and W.-H. Ip, Nature (London) **460**, 487 (2009).
[13] M. E. Brown and W. M. Calvin, Science **287**, 107 (2000); C. Dumas, R. J. Terrile, R. H. Brown, G. Schneider, and B. A. Smith, Astron. J. **121**, 1163 (2001).
[14] J. P. Emery, D. M. Burr, D. P. Cruikshank, R. H. Brown, and J. B. Dalton, Astron. Astrophys. **435**, 353 (2005); A. J. Verbiscer, D. E. Peterson, M. F. Skrutskie, M. Cushing, P. Helfenstein, M. J. Nelson, J. D. Smith, and J. C. Wilson, Icarus **182**, 211 (2006).
[15] L. J. Lanzerotti, W. L. Brown, K. J. Marcantonio, and R. E. Johnson, Nature (London) **312**, 139 (1984).
[16] M. J. Loeffler, U. Raut, and R. A. Baragiola, Astrophys. J. **649**, L133 (2006).
[17] G. Strazzulla and M. E. Palumbo, Planet. Space Sci. **46**, 1339 (1998).
[18] H. T. Smith, R. E. Johnson, E. C. Sittler, M. Shappirio, D. Reisenfeld, O. J. Tucker, M. Burger, F. J. Crary, D. J. McComas, and D. T. Young, Icarus **188**, 356 (2007).
[19] A. Blum, J. Chem. Soc., Faraday Trans. 1 **71**, 2299 (1975).
[20] W. Zheng, D. Jewitt, Y. Osamura, and R. Kaiser, Astrophys. J. **674**, 1242 (2008).
[21] G. Strazzulla, G. Leto, O. Gomis, and M. A. Satorre, Icarus **164**, 163 (2003).
[22] M. J. Loeffler, B. D. Teolis, and R. A. Baragiola, J. Chem. Phys. **124**, 104702 (2006).
[23] N. J. Sack and R. A. Baragiola, Phys. Rev. B **48**, 9973 (1993).
[24] www.srim.org
[25] M. J. Loeffler and R. A. Baragiola, J. Chem. Phys. **130**, 114504 (2009); M. J. Loeffler, U. Rauta, R. A. Vidala, R. A. Baragiola, and R. W. Carlson, Icarus **180**, 265 (2006).
[26] U. Raut, M. Famá, M. J. Loeffler, and R. A. Baragiola, Astrophys. J. **687**, 1070 (2008).
[27] U. Raut, B. D. Teolis, M. J. Loeffler, R. A. Vidal, M. Famá, and R. A. Baragiola, J. Chem. Phys. **126**, 244511 (2007).
[28] S. Suzer and L. Andrews, J. Chem. Phys. **89**, 5347 (1988).
[29] D. E. Milligan and M. E. Jacox, J. Chem. Phys. **43**, 4487 (1965).
[30] R. B. Bohn, S. A. Sandford, L. J. Allamandola, and D. P. Cruikshank, Icarus **111**, 151 (1994).
[31] R. A. Baragiola, Planet. Space Sci. **51**, 953 (2003).
[32] R. A. Haring, R. Pedrys, D. J. Oostra, A. Haring, and A. E. De Vries, Nucl. Instrum. Methods Phys. Res. B **5**, 476 (1984).
[33] J. W. T. Spinks and R. J. Woods, *An Introduction to Radiation Chemistry* (Wiley, New York, 1990).
[34] B. D. Teolis, J. Shi, and R. A. Baragiola, J. Chem. Phys. **130**, 134704 (2009).
[35] D. F. Strobel, Space Sci. Rev. **116**, 155 (2005).
[36] V. Buch and J. P. Devlin, J. Chem. Phys. **94**, 4091 (1991).
[37] U. Raut, M. Famá, B. D. Teolis, and R. A. Baragiola, J. Chem. Phys. **127**, 204713 (2007).
[38] R. E. Johnson and W. A. Jesser, Astrophys. J. **480**, L79 (1997).
[39] M. E. Palumbo, J. Phys.: Conf. Ser. **6**, 211 (2005).
[40] B. R. Cairns and G. C. Pimentel, J. Chem. Phys. **43**, 3432 (1965).
[41] B. D. Teolis, R. A. Vidal, J. Shi, and R. A. Baragiola, Phys. Rev. B **72**, 245422 (2005).
[42] J. F. Cooper, E. R. Christian, J. D. Richardson, and C. Wang, Earth, Moon, Planets **92**, 261 (2003); G. Strazzulla, J. F. Cooper, E. R. Christian, and R. E. Johnson, C. R. Phys. **4**, 791 (2003).
[43] E. M. Bringa, S. O. Kucheyev, M. J. Loeffler, R. A. Baragiola, A. G. G. M. Tielens, Z. R. Dai, G. Graham, S. Bajt, J. P. Bradley, C. A. Dukes, T. E. Felter, D. F. Torres, and W. van Breugel, Astrophys. J. **662**, 372 (2007).
[44] J. F. Cooper, P. D. Cooper, E. C. Sittler, S. J. Sturner, and A. M. Rymer, Planet. Space Sci. **57**, 1607 (2009).
[45] C. Paranicas, D. G. Mitchell, S. M. Krimigiss, D. C. Hamilton, E. Roussos, N. Krupp, G. H. Jones, R. E. Johnson, J. F. Cooper, and T. P. Armstrong, Icarus **197**, 519 (2008).
[46] S. Jurac, R. E. Johnson, J. D. Richardson, and C. Paranicas, Planet. Space Sci. **49**, 319 (2001).